



**Providing Choice & Value**

Generic CT and MRI Contrast Agents



**FRESENIUS  
KABI**

**CONTACT REP**

**AJNR**




**Correlation between Histopathology and  
Signal Loss on Spin-Echo T2-Weighted MR  
Images of the Inner Ear: Distinguishing  
Artifacts from Anatomy**

B.K. Ward, A. Mair, N. Nagururu, M. Bauer and B. Büki

This information is current as  
of July 22, 2025.

*AJNR Am J Neuroradiol* published online 1 September 2022  
<http://www.ajnr.org/content/early/2022/09/01/ajnr.A7625>

# Correlation between Histopathology and Signal Loss on Spin-Echo T2-Weighted MR Images of the Inner Ear: Distinguishing Artifacts from Anatomy

 B.K. Ward,  A. Mair,  N. Nagururu,  M. Bauer, and  B. Büki



## ABSTRACT

**BACKGROUND AND PURPOSE:** MR imaging of the inner ear on heavily T2-weighted sequences frequently has areas of signal loss in the vestibule. The aim of the present study was to correlate the anatomic structures of the vestibule with areas of low signal intensity.

**MATERIALS AND METHODS:** We reviewed T2-weighted spin-echo MR imaging studies of the internal auditory canal from 27 cases and cataloged signal intensity variations in the vestibulum of inner ears. Using a histologic preparation of a fully mounted human ear, we prepared 3D reconstructions showing the regions of sensory epithelia (semicircular canal cristae, utricular, and saccular maculae). Regions of low signal intensity were reconstructed in 3D, categorized by appearance, and compared with the 3D histologic preparation.

**RESULTS:** The region corresponding to the lateral semicircular canal crista showed signal loss in most studies (94%). In the utricle, a focus of signal loss occurred in the anterior-cranial portion of the utricle and corresponded to the location of the utricular macula and associated nerve on histopathologic specimens (63% of studies). Additional areas of low signal were observed in the vestibule, corresponding to the fluid-filled endolymphatic space and not to a solid anatomic structure.

**CONCLUSIONS:** Small foci of signal loss within the inner ear vestibule on T2-weighted spin-echo images correlate with anatomic structures, including the lateral semicircular canal crista and the utricular macula. More posterior intensity variations in the endolymphatic space are likely artifacts, potentially representing fluid flow within the endolymph caused by magneto-hydrodynamic Lorentz forces.

MR imaging of the temporal bone and lateral skull base has become common practice in the work-up of many clinical conditions, including sensorineural hearing loss, cholesteatoma, and infections of the lateral skull base. Increasingly, attention is being directed to the inner ear, for example in decisions about cochlear implant candidacy and in patients with Ménière disease.<sup>1-3</sup> The inner ear has been difficult to image with MR

imaging techniques due to its small size and environment, which includes a mixture of tissues of different proton densities, leading to susceptibility artifacts.<sup>4</sup> T2\*-weighted sequences using either gradient-echo (eg, CISS) or FIESTA are used at many centers but are prone to banding artifacts.<sup>5</sup> Other centers have used 3D fast spin-echo sequences (T2-weighted sampling perfection with application-optimized contrasts by using flip angle evolution [SPACE; Siemens]), which are less prone to magnetic susceptibility artifacts.<sup>6</sup>

In T2-weighted images generated using SPACE sequences, the labyrinthine fluids have a high signal intensity in sharp contrast with the low signal intensity of the surrounding bone of the otic capsule. The vestibule, however, is not entirely homogeneous, often showing patchy or filamentous areas of lower signal intensity. In the internal auditory canal, areas of low signal intensity on SPACE sequences are considered anatomic structures such as nerves and blood vessels. The increasing attention paid to inner ear structures on T2-weighted sequences prompted us to assess these areas of reduced signal intensity in the context of labyrinthine anatomy.

Received March 4, 2022; accepted after revision July 5.

From the Department of Otolaryngology-Head and Neck Surgery (B.K.W., N.N.), The Johns Hopkins University School of Medicine, Baltimore, Maryland; and Departments of Otolaryngology (A.M., B.B.) and Radiology (M.B.), Karl Landsteiner University Hospital Krems, Krems an der Donau, Austria.

B.K. Ward is supported by a clinician-scientist award K23DC018302 from the National Institutes of Health and by the Robert and Kate Niehaus Foundation. B. Büki is supported by the grants RTO005 and SF06 from the Karl Landsteiner Private University of Health Sciences, Krems an der Donau, Austria.

Please address correspondence to Béla Büki, MD, Department of Otolaryngology, Karl Landsteiner University Hospital Krems, Mitterweg 10, 3500 Krems an der Donau, Austria; e-mail: bela.bueki@krems.lknoe.at

 Indicates open access to non-subscribers at [www.ajnr.org](http://www.ajnr.org)

<http://dx.doi.org/10.3174/ajnr.A7625>

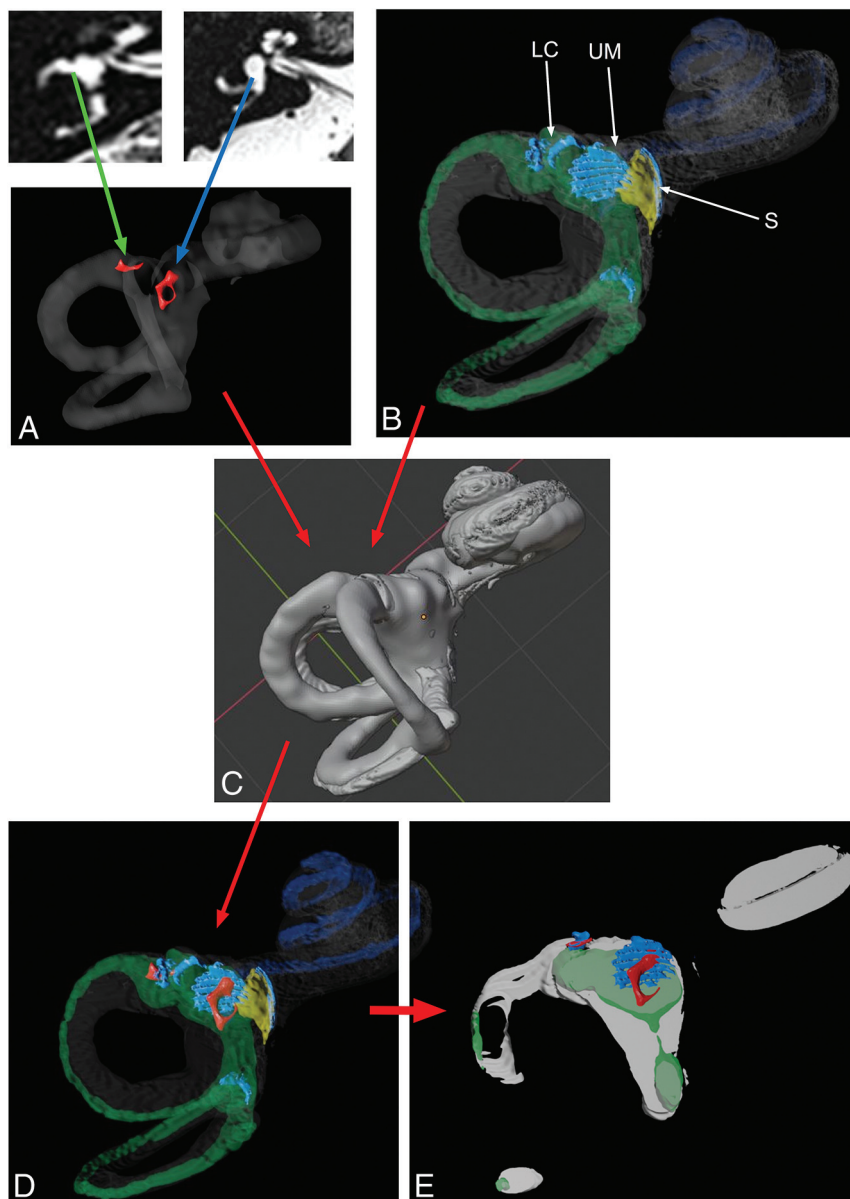


**FIG 1.** Demonstration of a morphologic fitting procedure, which was applied to search for correlations between MR images and anatomy observed in histologic sections. *A*, Inner ear fluid-filled spaces (right ear) as seen in the SPACE images were reconstructed in 3D (the 3D reconstruction has been mirrored to fit the anatomy of the left ear). Red: Note 2 landmarks in the MR images: an indentation in the region of the lateral canal crista (green arrow) and a diamond-shaped area of low signal (blue arrow). *B*, 3D reconstruction of the histologic sections (left ear) showing the lateral canal crista (LC), utricular macula (UM), and saccular macula (S). *C*, The two 3D reconstructions (MR imaging and histology) are fitted together according to their outer (perilymphatic) fluid boundary. *D*, Results of the fitting (green: histologic endolymphatic space of the utricle and semicircular canals). *E*, The composite fitted MR imaging and histologic 3D compartments are re-sectioned in the plane of the MR imaging sections to create a virtual MR image based on histology in which the regions with low signal intensity are embedded. In this image, the indentation in the region of the lateral canal crista on MR imaging (red) is colocalized with the same structure from histology (blue) and the diamond-shaped area shown in red projected more cranially to the utricular macula (blue).

Our aim in this retrospective study was to classify these foci of low signal intensity within the vestibulum according to their topography and to determine whether they correspond to anatomic structures.

## MATERIALS AND METHODS

### Research Design and Patients/Subjects

In this retrospective study, we reviewed T2-weighted SPACE sequence MR images from patients who were examined at the Department of Otolaryngology, Karl Landsteiner University Hospital Krems, Krems an der Donau, Austria, between January 1, 2019, and June 30, 2020. The study had been authorized by the Bioethics Committee of Lower Austria (GS4-EK-4/676-2020). All patients were older than 18 years of age, and in all cases, the radiologic evaluation showed normal high signal intensity representing the fluid-filled spaces of the inner ear, including the cochlea, vestibule, and semicircular canals.

### MR Imaging Data Acquisition and Processing

The SPACE technique consists of a 3D-fast (turbo) spin-echo acquisition using very long echo-train lengths (typically 100–250 echoes), ultrashort echo spacing (typically 3–4 ms), nonselective refocusing pulses, and reduced flip angles. The examinations used a Magnetom Verio 3T MR imaging system (Siemens) with the following sequence parameters: TR, 1000 ms; TE, 135 ms; section thickness, 0.5 mm; bandwidth, 289 Hz/pixel; flip angle, 120°; echo spacing, 6.84 ms.

The MR imaging SPACE sequences were evaluated independently by 2 investigators for foci of low signal intensity in the vestibule without any processing using the DICOM viewer MagicView DANUBE (Siemens). Images were exported as JPEGs, and a scalar volume was created using Slicer (Version 4.10.2; <http://www.slicer.org>). The areas of low signal intensity in the vestibule were manually defined and registered in Slicer. The MR images were then three-dimensionally reconstructed (as illustrated in Fig 1A).

### Processing of the Histology Sections

One normal ear (left side) from the temporal bone collection of the Otopathology

Laboratory at the Massachusetts Eye and Ear Infirmary was examined (National Institute on Deafness and Other Communication Disorders National Temporal Bone Registry; institutional review board ethical commission permission number: 92-04-017X). The

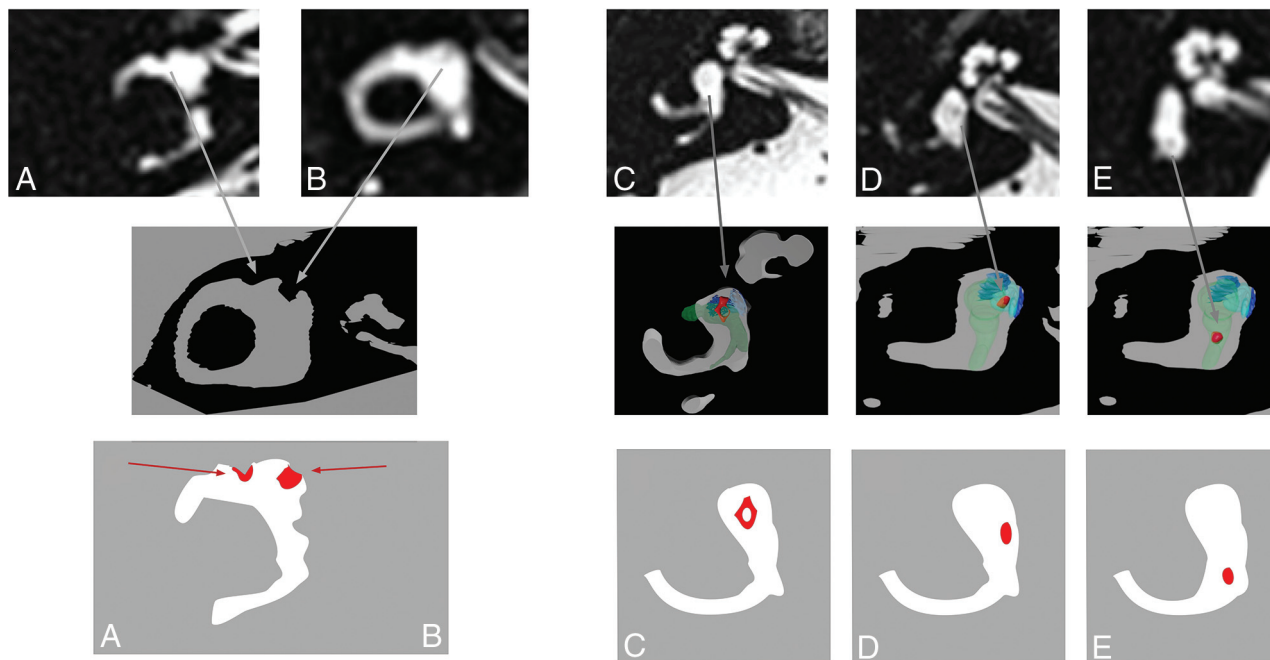


**FIG 2.** Landmarks identified in the MR images (*upper row*) and in the histologic images (*middle row*; red: foci of low intensity from the MR imaging projected into the histologic section after the 3D fitting procedure). Red: MR imaging hypointensities reconstructed in 3D. Dark blue: utricular macula. Transparent green: endolymphatic space. Light blue, saccule (for an explanation also see D). *Lower row*: Schematic drawing depicting the 5 areas of interest. A, Lateral canal crista. B, Utricular root region. C, Utricular “diamond.” D, Focus of low intensity in the posterior vestibulum. E, Focus of low intensity in the saccular region. Red: ROIs, statistically evaluated.

donor was a 71-year-old man, and the specimen was acquired 14 hours postmortem. The ear was horizontally sectioned (ie, in the axial plane) with a section thickness of 20  $\mu$ m with every section stained with H&E and mounted. The histologic slides were scanned using an Aperio AT2 scanner and viewed using Aperio ImageScope (Leica Biosystems). The ROIs were captured using a resolution of 3264  $\times$  1836 and stored in JPEG format. Anatomic details such as the lateral canal crista, utricular macula, and saccular macula were manually defined and registered in Slicer. The 440 images were manually aligned using Fiji ImageJ (National Institutes of Health, Bethesda) and three-dimensionally reconstructed using Slicer<sup>7</sup> (as illustrated in Fig 1B). By means of Blender 2.82 (<https://www.blender.org/download/releases/2-82/>), a composite 3D model of the temporal bone histology including membranous spaces was built and virtually re-sectioned in the plane of the MR image sections. This process was necessary because the histologic sections are much thinner than the MR image slices, and the radiologic plane differed from the plane of the histologic sections.

#### Preliminary Fitting of the MR Images to the Histology

After the 3D reconstruction of the histologic sections was completed, the 3D MR imaging and 3D histology were scaled and fit. Using Blender, the location of the areas of low signal intensity on MR imaging were compared with the anatomic details from the reconstructed histology of the inner ear (Fig 1). After patterns of low signal intensity were identified, to focus on normal anatomy, we excluded patients with a diagnosis of a peripheral vestibular disorder from the final analysis.

#### Statistical Methods

The frequency of observation of areas of low signal intensity was compared between the left and right inner ears using a Fisher exact test. Statistical analyses were performed using Graph Pad Prism, Version 5.03 for Windows (GraphPad Software). A *P* value < .05 was considered statistically significant.

#### RESULTS

Originally 43 cases were identified that met the inclusion criteria. After a preliminary examination of the MR images for regions of low signal intensity, 5 patterns of low signal intensity in the vestibule were identified (Fig 2): 1) a focus near the anterior takeoff of the lateral semicircular canal; 2) the anterior-cranial part of the vestibule we called the utricular root; 3) a rhomboid or diamond-shaped filamentous area of decreased signal within the middle portion of the vestibule; 4) a focus near the saccule (saccular region); and 5) a focus in the posterior vestibule. The MR imaging SPACE sequences were evaluated independently by 2 investigators and the interrater agreement for identifying the regions of low signal intensity for the 2 examiners was 97.9% (Cohen  $\kappa$  = 0.907).

After the classification of these ROIs, 5 cases with the clinical diagnosis of vestibular neuritis, 3 cases with Ménière disease, and 8 cases with benign paroxysmal positional vertigo were excluded from the analysis because we intended to focus on normal peripheral vestibular anatomy. Ultimately, scans from 27 patients (13 women, 14 men) were processed (average age, 63 years; range, 35–89 years). Clinical diagnoses were hypertensive crisis (*n* = 3), idiopathic sudden hearing loss (*n* = 12), tinnitus (*n* = 2), central downbeat nystagmus (*n* = 1), minor cerebral hemorrhage

## Frequency of foci of low signal intensity among vestibular ROIs

	ROIs (No.)				
	Lateral Semicircular Canal Crista	Utriclar Root Region	Utriclar "Diamond"	Saccular Region	Posterior Vestibular Region
Right side	25/27 (93%)	17/27 (63%)	23/27 (85%)	0/27 (0%)	25/27 (93%)
Left side	26/27 (96%)	17/27 (63%)	13/27 <sup>a</sup> (48%)	0/27 (0%)	20/27 (74%)

<sup>a</sup> Significant difference between left and right sides (Fisher exact test, 2-tailed *P* value = .0084).

(*n* = 1), subependymal tumor (*n* = 1), migraine (*n* = 1), transient ischemic attack (*n* = 2), trigeminal neuralgia (*n* = 1), syncope (*n* = 2), and vestibular schwannoma (*n* = 1).

The Table shows the frequency of the areas of low signal intensity for the left and right inner ears. The indentation caused by low signal intensity near the anterior takeoff of the lateral semicircular canal corresponded, on histology, to the lateral semicircular canal crista and was found in 93% of the right ears and in 96% of the left ears (Fig 2A). A signal loss adjacent to the anterior-superior part of the bony vestibule corresponded to the attachment or "root" of the utricular macula and could be seen in 63% of both left and right inner ears (Fig 2B). The remaining 3 areas of low signal intensity within the vestibule did not correspond to solid anatomic structures on the histologic specimen. The rhomboid or diamond-shaped area of reduced signal in the middle of the vestibule was observed with variable frequency for the inner ears on both sides, being significantly more commonly seen in the right inner ear than in the left (85% versus 48%, significant by the Fisher exact test; the 2-tailed *P* value = .0084) (Fig 2C). The low signal around the anatomic location of the sacculle was not found in the final group of examined ears. The regions of low signal intensity were decided before excluding cases of peripheral vestibular disorders (Materials and Methods). There was 1 right ear in which a focus of low signal intensity was seen in this saccular region, and this case was excluded because of the diagnosis of ipsilateral benign paroxysmal positional vertigo (Fig 2D). In the more posterior-caudal region of the vestibule a small, round focus of low signal intensity was seen in 93% of right ears and 74% of the left inner ears (not significantly different by the Fisher exact test; the 2-tailed *P* value = .1415) (Fig 2E). The diamond-shaped area of low signal in the middle of the vestibule and the small round gray area in the posterior-caudal vestibule projected into the fluid-filled endolymphatic spaces on histology (Fig 2C, -D).

## DISCUSSION

In this study, by comparing conventional spin-echo T2-weighted images with a detailed 3D histologic reconstruction of inner ear anatomy, we found 2 inner ear anatomic structures that can be identified frequently by reduced signal intensity and 2 areas of low signal that do not correspond to a solid anatomic structure. An indentation is found consistently on both right and left inner ears at the anterior attachment of the lateral semicircular canal to the vestibule, corresponding to the anatomic position of the lateral semicircular canal crista. More medially and somewhat caudal from the crista, foci of low signal intensity were observed in more than half of the cases on both sides approximately at the anatomic position of the root of the utricular macula. The bulk of

the utricular root spreads over 400  $\mu$ m along the z-axis (ie, 20 histologic slices), and the section thickness of the MR images was 500  $\mu$ m, which means that this tiny tissue mass protruding into the fluid-filled vestibule may have been missed due to partial volume averaging, with the high signal intensity of the surrounding fluid perhaps accounting for its being found only in 63% of the ears.

The frequency by which the root of the utricular macula could be seen was exactly the same on the left and right sides, supporting the hypothesis that the signal loss corresponds to an anatomic structure.

The additional 2 areas of low signal intensity within the vestibule did not correlate with solid anatomic structures but rather corresponded to regions of the endolymph-filled space of the vestibule on histology. The inner ear houses a thin membranous labyrinth that contains potassium-enriched fluid called endolymph and is surrounded by sodium-enriched perilymph. The sensory epithelia of the inner ear are located within the endolymph-filled space of the membranous labyrinth. The composition of these fluids is like water, indicating that endolymph and perilymph ought to have similar proton density and therefore a similar signal intensity on T2-weighted spin-echo images. The loss of signal within this space is likely an artifact.

An advantage of T2-weighted spin-echo sequences like SPACE over T2\*-weighted gradient-echo sequences is fewer magnetic susceptibility artifacts.<sup>8</sup> T2-weighted TSE sequences like SPACE, however, are especially susceptible to movement artifacts.<sup>9</sup> The imaging characteristics of CSF cause it to manifest as intense signal on T2-weighted images.<sup>10</sup> The loss of signal, caused, for instance, when protons in fluid move during image acquisition, is called a flow void. Although considered an artifact, flow void has been used to examine the movement of the CSF in cases with normal-pressure hydrocephalus.<sup>11-14</sup> Areas of low signal intensity within the CSF can be caused by CSF flow-related phenomena and are divided into 2 categories: time-of-flight (TOF) effects and phase-related effects from turbulent flow, with turbulent flow creating greater loss of signal.<sup>10</sup>

Previously, the inner ear was modelled as a closed system with relatively little fluid flow. Increasingly, however, attention is being paid to flow phenomena in the inner ear.<sup>15</sup> In 2011, Roberts et al<sup>16</sup> discovered that healthy humans have a beating of the eyes called nystagmus in MR imaging machines of at least 3T. They reported nystagmus in all (*n* = 10) of their healthy human volunteers with the effect being greater at 7T than at 3T magnetic fields. The authors proposed that the effect is caused by a magneto-hydrodynamic Lorentz force occurring in the inner ear vestibule, induced by the interaction of normal ionic currents entering utricle hair cells and the strong static magnetic field of the MR imaging machine.<sup>16,17</sup> The Lorentz force has been attributed primarily to the ionic currents within endolymph associated with the utricle, though the effect would not be on the utricle macula and hair cells themselves but through the movement of the endolymph into the nearby openings of the lateral and superior semicircular canals, pushing on the cupulae and producing a nystagmus.<sup>17</sup> The nystagmus effect

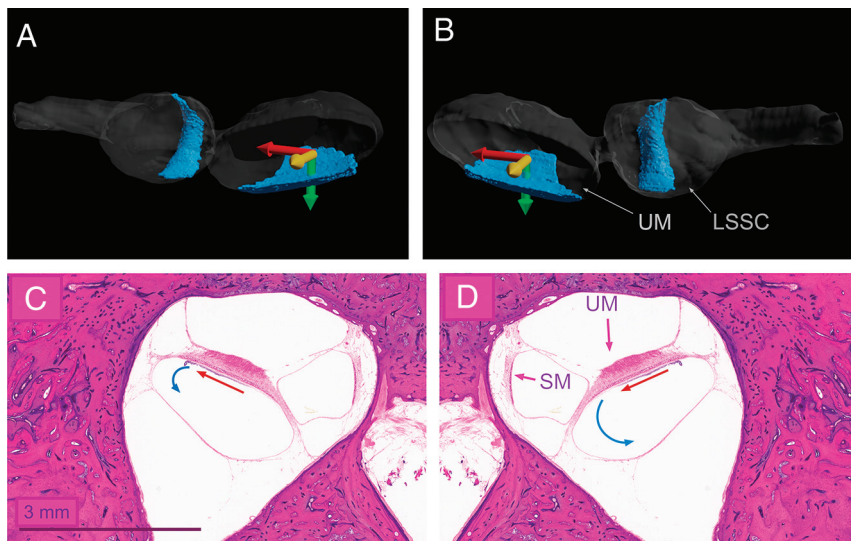


**FIG 3.** Cartoon presentation of the hypothetical mechanism of asymmetric turbulent fluid movements in the left and right ears caused by Lorentz forces. The Lorentz force (red arrow) is evoked, the direction determined by the right-hand rule, by the combination of the magnetic field (yellow arrow) and the utricle current (green arrow) as described in Roberts et al.<sup>16</sup> The anterior part of the utricle and lateral semicircular canal viewed from posterior on the left (A) and right (B) side. 3D reconstruction of the endolymphatic space from the histologic specimen. UM indicates utricular macula; LSSC, lateral semicircular canal crista in the ampulla. C and D, Original axial histologic section of the left inner ear across the utricular macula. Image C was mirrored horizontally to create the impression of the right inner ear. UM indicates utricular macula; SM, saccular macula; red arrows, magneto-hydrodynamic Lorentz force; blue arrows, hypothetical turbulent endolymph movements.

persists the entire time the person lies within the static magnetic field, physiology that could only occur if there was a continuous fluid flow constantly displacing the semicircular canal cupulae. On the 3D reconstruction in this study, additional foci of low signal were located within the endolymph space, both cranial to the utricular root and in the posterior vestibule, the first of which corresponds directly to the location of endolymphatic fluid vortices that could cause the nystagmus observed in MR imaging machines.

We hypothesized that the 2 foci of low signal within the vestibule that do not correlate with anatomic structures are caused by local endolymph movement. Low signal from TOF effects occurs in spin-echo imaging like SPACE sequences when protons do not experience both the initial radiofrequency pulse and the subsequent radiofrequency refocusing pulse. Turbulent flow results in a broader spectrum of proton velocities and a wide range of flow directions that are not seen in laminar flow. The varied flow velocities and directions result in more rapid dephasing and signal loss, termed “intravoxel dephasing.”<sup>10,18</sup> TOF effects are also more pronounced (lower signal) with faster proton velocity, thinner slices, longer TEs, and an imaging plane perpendicular to flow.<sup>10</sup> In our case, the section thickness was 0.5 mm; the TE was long at 135 ms; and the imaging plane was perpendicular to the hypothetical flow direction (Fig 3). The frequency of these putative flow void artifacts was different between the ears on the left and right sides, potentially related to the mirrored anatomy across the ears, yet with the identical direction of flow based on the mechanism of the

Lorentz force. These factors all may have augmented the flow artifacts even with a relatively slow-but-turbulent flow in the vestibule.

A limitation of the study is that only 1 normal cadaveric temporal bone was fully processed and reconstructed to compare with the MR images of the study population. Observations from the cadaver may not correlate perfectly with findings in the imaged patients. The spatial resolution of a 3D reconstructed, fully processed cadaveric specimen exceeds that of standard histologic preparations, and due to the time-intensive process of digitizing and manually aligning the specimen, few fully processed specimens have been reported in the literature.<sup>19,20</sup> Nevertheless, on the basis of the appearance of normal labyrinthine fluid spaces from other lower-resolution specimens, we are confident that the specimen used in this study represents a typical distribution of the different scalar volumes in a normal specimen.

In this study, we excluded cases in which pathology may have affected the peripheral vestibular system. The aim was to describe the findings in the normal inner ear; however, the included

participants all had a clinical indication for the imaging study that may have affected the frequency of the observed findings. Nevertheless, the findings may have implications for patients who could demonstrate different patterns of low signal intensity, as in the single case in which low signal was seen near the saccule in an individual with ipsilateral benign paroxysmal positional vertigo but in none of the cases without a peripheral vestibular disorder. In cases with utricular endolymphatic hydrops, flow void artifacts may appear differently compared with normal ears. Changes in inner ear signal intensity, for instance in cases with dysfunction of the utricular macula (vestibular neuritis) or intralabyrinthine schwannoma, could benefit from more precise localization of affected inner ear structures. More precise localization of signal abnormalities can aid clinicians treating patients with inner ear abnormalities.

## CONCLUSIONS

In this study, we identified foci of low signal intensity in the vestibule in T2-weighted spin-echo MR images. While some areas of low signal corresponded on histology to structures like the lateral semicircular canal crista and the utricular macula, others corresponded to the fluid-filled endolymphatic space of the utricle. We hypothesize that these latter areas are artifacts caused by fluid movements in the endolymphatic space and could result from magneto-hydrodynamic Lorentz forces.

## ACKNOWLEDGMENTS

The authors thank Joseph B. Nadol Jr and MengYu Zhu from the National Institute on Deafness and Other Communication Disorders National Temporal Bone, Hearing and Balance Pathology Registry Resource (U24DC013983-01) for access to the histologic preparations and for their support in 2020. We also thank Margit Kirschbaum for her technical help and are grateful for the dedicated work of 3 anonymous reviewers.

Disclosure forms provided by the authors are available with the full text and PDF of this article at [www.ajnr.org](http://www.ajnr.org).

## REFERENCES

1. Lopez-Escamez JA, Attye A. Systematic review of magnetic resonance imaging for diagnosis of Meniere disease. *J Vestib Res* 2019;29:121–29 [CrossRef Medline](#)
2. Pyrkko I, Zou J, Poe D, et al. Magnetic resonance imaging of the inner ear in Meniere's disease. *Otolaryngol Clin North Am* 2010;43:1059–80 [CrossRef Medline](#)
3. Gerb J, Ahmadi SA, Kierig E, et al. VOLT: a novel open-source pipeline for automatic segmentation of endolymphatic space in inner ear MRI. *J Neurol* 2020;267:185–96 [Medline](#)
4. Oehler MC, Schmalbrock P, Chakeres D, et al. Magnetic susceptibility artifacts on high-resolution MR of the temporal bone. *AJNR Am J Neuroradiol* 1995;16:1135–43 [Medline](#)
5. Lane JJ, Ward H, Witte RJ, et al. 3-T imaging of the cochlear nerve and labyrinth in cochlear-implant candidates: 3D fast recovery fast spin-echo versus 3D constructive interference in the steady state techniques. *AJNR Am J Neuroradiol* 2004;25:618–22 [Medline](#)
6. Naganawa S, Koshikawa T, Fukatsu H, et al. MR cisternography of the cerebellopontine angle: comparison of three-dimensional fast asymmetrical spin-echo and three-dimensional constructive interference in the steady-state sequences. *AJNR Am J Neuroradiol* 2001;22:1179–85 [Medline](#)
7. Fedorov A, Beichel R, Kalpathy-Cramer J, et al. 3D Slicer as an image computing platform for the Quantitative Imaging Network. *Magn Reson Imaging* 2012;30:1323–41 [CrossRef Medline](#)
8. Mugler JP, 3rd, Bao S, Mulkern RV, et al. Optimized single-slab three-dimensional spin-echo MR imaging of the brain. *Radiology* 2000;216:891–99 [CrossRef Medline](#)
9. Ucar M, Guryildirim M, Tokgoz N, et al. Evaluation of aqueductal patency in patients with hydrocephalus: three-dimensional high-sampling-efficiency technique (SPACE) versus two-dimensional turbo spin echo at 3 Tesla. *Korean J Radiol* 2014;15:827–35 [CrossRef Medline](#)
10. Lisanti C, Carlin C, Banks KP, et al. Normal MRI appearance and motion-related phenomena of CSF. *AJR Am J Roentgenol* 2007;188:716–25 [CrossRef Medline](#)
11. Kartal MG, Algin O. Evaluation of hydrocephalus and other cerebrospinal fluid disorders with MRI: an update. *Insights Imaging* 2014;5:531–41 [CrossRef Medline](#)
12. Bradley WG Jr, Scalzo D, Queralto J, et al. Normal-pressure hydrocephalus: evaluation with cerebrospinal fluid flow measurements at MR imaging. *Radiology* 1996;198:523–29 [CrossRef Medline](#)
13. Sherman JL, Citrin CM. Magnetic resonance demonstration of normal CSF flow. *AJNR Am J Neuroradiol* 1986;7:3–6 [Medline](#)
14. Algin O, Turkbey B, Ozmen E, et al. Evaluation of spontaneous third ventriculostomy by three-dimensional sampling perfection with application-optimized contrasts using different flip-angle evolutions (3D-SPACE) sequence by 3T MR imaging: preliminary results with variant flip-angle mode. *J Neuroradiol* 2013;40:11–18 [CrossRef Medline](#)
15. Obrist D. Flow phenomena in the inner ear. *Annu Rev Fluid Mech* 2019;51:487–510 [CrossRef](#)
16. Roberts DC, Marcelli V, Gillen JS, et al. MRI magnetic field stimulates rotational sensors of the brain. *Curr Biol* 2011;21:1635–40 [CrossRef Medline](#)
17. Ward BK, Roberts DC, Otero-Millan J, et al. A decade of magnetic vestibular stimulation: from serendipity to physics to the clinic. *J Neurophysiol* 2019;121:2013–19 [CrossRef Medline](#)
18. Bradley WG Jr. Carmen lecture: flow phenomena in MR imaging. *AJR Am J Roentgenol* 1988;150:983–94 [CrossRef Medline](#)
19. Buki B, Mair A, Pogson JM, et al. Three-dimensional high-resolution temporal bone histopathology identifies areas of vascular vulnerability in the inner ear. *Audiol Neurotol* 2022;27:249–59 [CrossRef Medline](#)
20. Buki B, Ward BK. Length of the narrow bony channels may not be the sole cause of differential involvement of the nerves in vestibular neuritis. *Otol Neurotol* 2021;42:e918–24 [CrossRef Medline](#)